SCIENTIFIC REPORTS

OPEN

Improving the electrochemical performances using a V-doped Ni-rich NCM cathode

Received: 27 March 2019
Accepted: 6 June 2019
Published online: 20 June 2019

Seoung-Ju Sim, Seung-Hwan Lee, Bong-Soo Jin & Hyun-Soo Kim

Ni-rich layered $LiNi_{0.84}Co_{0.10}Mn_{0.06}O_2$ cathode material was modified by doping with vanadium to enhance the electrochemical performances. The XRD, FESEM and XPS analyses were indicated that the vanadium is successfully doped in the crystal lattice of $LiNi_{0.84}Co_{0.10}Mn_{0.06}O_2$ with high crystallinity. 0.05 mol% vanadium doped $LiNi_{0.84}Co_{0.10}Mn_{0.06}O_2$ exhibits superior initial discharge capacity of 204.4 mAh g^{-1}, cycling retention of 88.1% after 80 cycles and rate capability of 86.2% at 2 C compared to those of pristine sample. It can be inferred that the vanadium doping can stabilize the crystal structure and improve the lithium-ion kinetics of the layered cathode materials.

Lithium-ion batteries (LIBs) are being widely used for portable device, uninterruptible power supplies (UPS), hybrid electric vehicles (HEVs), electric vehicles (EVs) and so on. The recent demand for LIBs has been considerably increasing and the research for LIBs focuses on high capacity, long cycle life and high-rate capability. Recently, Ni-rich layered oxide has received a lot of attention due to their higher specific capacity, lower cost and lower toxic than other cathode materials[1]. However, the long-term cycling stability is proportionally deteriorated with increasing Ni contents. It can be caused by surface side reactions, phase transitions during charge-discharge, the reduction of Ni^{4+} and oxygen release, resulting in deterioration the crystal structure. This phenomenon suffers a decrease in electrochemical performance, and hinder commercialization[2,3].

Many efforts have been made to solve these problems and modify cathodes using coatings[4], dopants[5], core-shell[6], concentration-gradient structures[7] and single crystalline materials[8,9]. Among them, doping is an effective strategy to improve stability of layered structure because the dopant ions help suppression of the phase transition and the voltage fading. So far, lots of single dopants have been explored such as Al[10], Ti[11], Zr[12], Mg[13], Mo[14], Na[15], Sn[16], B[17], Fe[18] and Cr[19] to improve the electrochemical performance of layered cathode materials. Vanadium was also studied as one of the dopant by many researchers because vanadium can take various valence state, leading to the stability of the crystal and increase of Li-ion diffusion coefficient[20–23]. These can significantly improve the capacity, coulombic efficiency, cycleability and rate capability. To the best of our knowledge, the effect of the vanadium doped Ni-rich NCM have still not been studied.

Therefore, in this paper, we synthesized well-crystallized V-doped Ni-rich $LiNi_{0.84}Co_{0.10}Mn_{0.06}O_2$ (hereafter V-doped NCM) by solid state method to stabilize the crystal structure and deliver superior electrochemical performances.

Experimental Section

For the synthesis of $LiNi_{0.84}Co_{0.10}Mn_{0.06}O_2$, the $Ni_{0.84}Co_{0.10}Mn_{0.06}(OH)_2$ precursor was prepared by a co-precipitation method. An aqueous solution of $NiSO_4{\cdot}6H_2O$, $CoSO_4{\cdot}7H_2O$ and $MnSO_4{\cdot}H_2O$ was used as starting materials. Simultaneously, a NaOH solution and NH_4OH solution as a chelating agent were also used. The prepared spherical $Ni_{0.84}Co_{0.10}Mn_{0.06}(OH)_2$ precursor was mixed with $LiOH{\cdot}H_2O$ at a molar ratio of 1: 1.05 and V_2O_5 powder as a vanadium source with the molar ratios of 0, 0.005, 0.01 and 0.02 mol%. After that, the powders were calcined at 500 °C for 5 h and 760 °C for 15 h in air. V-doped NCM was prepared as illustrated in Fig. 1.

The crystal structure of the materials was characterized by X-ray diffraction (XRD, X-pert PRO MPD, Philips, Cu Kα), in the 2θ range of 10°–80°. The morphology of the samples was observed by field emission scanning electron microscopy (FESEM, S-4800, HITACHI) and elemental mappings of the samples were measured by an energy dispersive X-ray detector (EDX, X-maxN, HORIBA). The chemical state of transition was conducted by X-ray photoelectron spectroscopy (XPS, VG SCIENTIFIC, ESCALAB 250, Al Kα radiation).

Next-Generation Battery Research Center, Korea Electrotechnology Research Institute, Changwon, 641-120, South Korea. Seoung-Ju Sim and Seung-Hwan Lee contributed equally. Correspondence and requests for materials should be addressed to H.-S.K. (email: hskim@keri.re.kr)

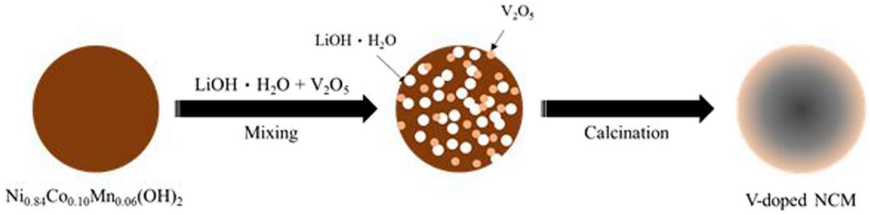

Figure 1. Schematic illustration of the synthesis process of V-doped NCM.

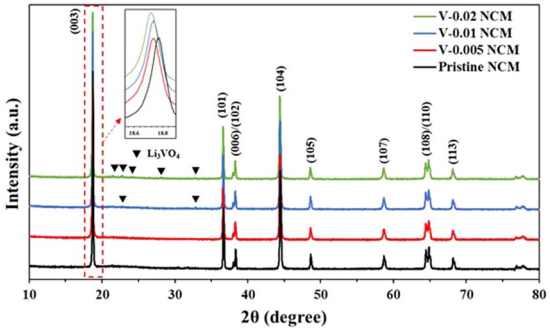

Figure 2. XRD patterns of pristine and V-doped NCM samples.

For the electrochemical performance, the cathode electrode was prepared by mixing 96 wt% active material, 2 wt% super P and 2 wt% polyvinylidene fluoride (PVDF) binder. The mixed slurry was coated on Al foil (16 μm in thickness) and dried at 100 °C for 10 h in a vacuum oven. After that, the electrode was punched into disks and then dried at 120 °C for 10 h. A 2032 coin cells were fabricated with pristine and V-doped NCM as a cathode and lithium foil (500 μm in thickness) as an anode. A polyethylene (PE, 20 μm in thickness) was used as a separator and 1 M $LiPF_6$ in a mixed solution containing ethylene carbonate (EC)/dimethyl carbonate (DMC)/ethylmethyl carbonate (EMC) (1:1:1, v/v/v) was employed as electrolyte. The assembly of all coin cells was carried out in an argon-filled glove box.

Charge-discharge test was carried out galvanostatically under the voltage range of 3.0–4.3 V and various current density using electrochemical equipment (TOSCAT-3100, Toyo system) at 25 °C. Cyclic voltammetry (CV) of the samples was carried out by multi potentiostat (VSP300, Bio-Logic) between 3.0 and 4.3 V at a scan rate of 0.1 mV s^{-1}. The electrochemical impedance spectroscopy (EIS) measurement was conducted with a VSP300 impedance analyzer using the frequency range of 1 MHz to 10 mHz with 5 mV amplitude.

Results and Discussion

The XRD patterns of pristine and V-doped NCM are shown in Fig. 2. The patterns are indexed based on a layered hexagonal α-$NaFeO_2$ structure with the space group R-3m[24]. It can be inferred that V-doped NCM maintains the crystal structure of pristine NCM since XRD patterns of V-doped NCM are similar to that of pristine NCM due to low doping concentration[25,26]. The V-doped NCM has a clear peak splitting of the (006)/(102) and (108)/(110), indicating well-ordered layered structure[27]. The (003) peak shifts to lower angle with increasing V content by Bragg's law ($n\lambda = 2d\sin\theta$), indicating vanadium was successfully incorporated into the NCM cathode. It can be inferred that the V^{5+} ions, having larger ionic radius (0.59 Å) than those of Ni^{2+} (0.56 Å), Co^{3+} (0.54 Å) and Mn^{4+} (0.53 Å), were substituted into the lattice of the NCM[28]. It can also be explained by charge compensation that dopant can change the valence states of transitional metal with different ionic radii via vanadium doping[29]. Therefore, the lattice parameters increase linearly with an increase in doping concentration, enabling smooth and fast kinetics of Li ions[30]. The $I_{(003)/(104)}$ ratio indirectly means the degree of cation mixing in the layered structure, resulting from similar ionic radius of Li^+ (0.76 Å) and Ni^{2+} (0.69 Å)[31]. There is a little difference in the $I_{(003)/(104)}$ ratios and the ratios of pristine, 0.005 mol% (V-0.005 NCM), 0.01 mol% (V-0.01 NCM) and 0.02 mol% (V-0.02 NCM) doped NCM were 1.31, 1.35, 1.29 and 1.25, respectively. The V-0.005 NCM shows the highest $I_{(003)/(104)}$ ratio of 1.35, indicating the low cation mixing with lithium ions at the 3a site, transition-metal ions at the 3b site[32]. We can assume that the cation mixing is decreased by replacing Ni in NCM with V, beneficial to Li ion diffusion. However, excessive V doping above 0.01 mol% shows a lower $I_{(003)/(104)}$ ratio, indicating high Li^+/Ni^{2+} cation mixing, since it can lead to deformation of the NCM original structure[30]. Therefore, we can infer that suitable vanadium substitution can reduce the Li/Ni cation mixing with well-ordered layered structure.

Figure 3 shows the FESEM images of the pristine and V-doped NCM samples. All powders show a similar spherical morphology and no great difference between the samples. The spherical samples are composed of numerous primary particles. The primary particles have similar size (500 nm) regardless of the vanadium doping level. We can infer that vanadium doping do not affect the morphology and size of NCM materials. The porous structure of spherical NCM enables to rapid Li ion kinetics, derived from sufficiently soaked liquid electrolyte[33].

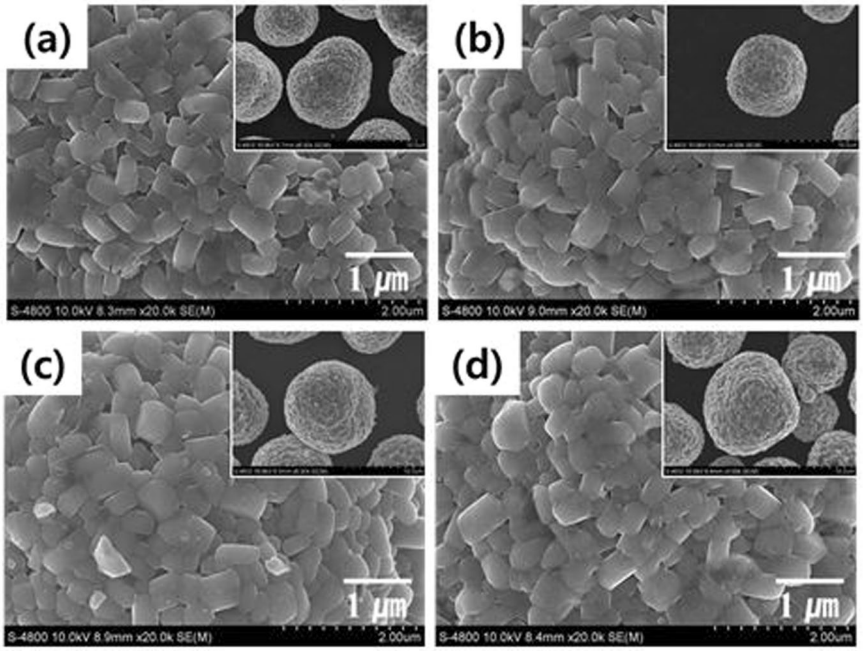

Figure 3. FESEM images of pristine and V-doped NCM samples: (**a**) pristine, (**b**) V-0.005 M, (**c**) V-0.01 M, and (**d**) V-0.02 M.

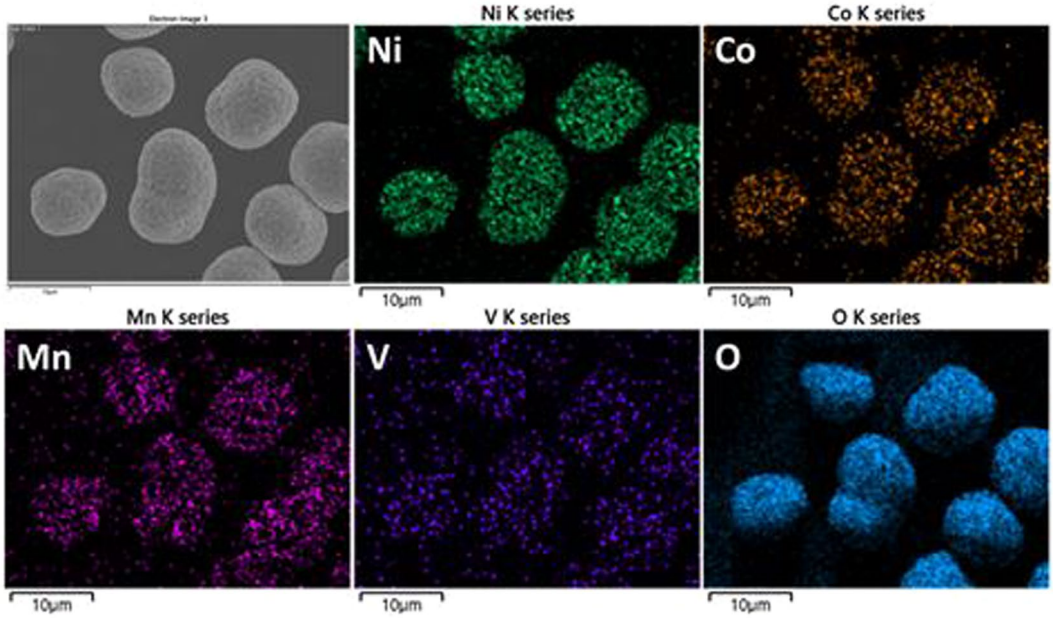

Figure 4. EDX mapping images of V-doped NCM sample.

Figure 4 shows EDX mapping of V-0.005 NCM to confirm the presence of doped vanadium within the NCM. It can be seen that the elements of Ni, Co, Mn, V and O were uniformly distributed in the sample since there is no agglomeration and void region in the mapping of vanadium.

XPS analysis was performed to gain further information of composition and the chemical state of V-doped NCM. The XPS spectra of pristine and V-0.005 NCM are shown in Fig. 5 to confirm the valance states of transition metal elements (Ni, Co, Mn and V). The Ni, Co and Mn elements have almost similar binding energy before and after V-doped NCM. The Ni2p spectra of samples are characterized by $Ni2p_{3/2}$ and $Ni2p_{1/2}$. The $Ni2p_{3/2}$ peak appears at 855.8 eV, which means a high oxidation state[34,35]. The binding energies of $Co2p_{3/2}$, $Co2p_{1/2}$ appear at 781.8 eV, 795.4 eV, indicating the dominant Co^{3+} cation. The Mn spectrum has the binding energy of 644.3 eV for the $Mn2p_{2/3}$, indicating Mn^{4+} cation[36]. It agrees with the previous report for the NCM cathode materials[37]. Although no peaks corresponding to dopant vanadium are observed at the XRD (Fig. 2) due to its small amount,

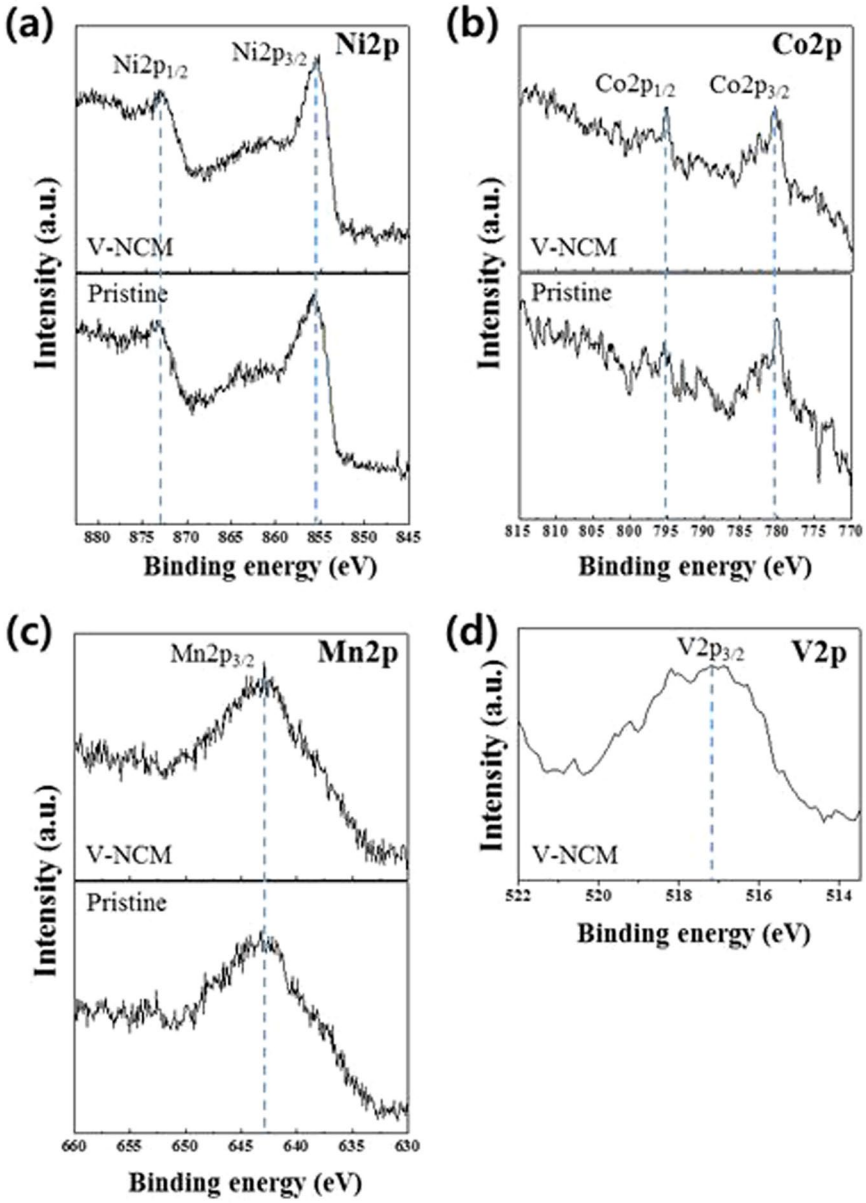

Figure 5. XPS spectra of (**a**) Ni2p, (**b**) Co2p, (**c**) Mn2p and (**d**) V2p for pristine and V-doped NCM samples.

it was confirmed by XPS analysis. The binding energy value of $Vp_{3/2}$ was detected at 517.2 eV, which implies that the valance of vanadium is a high oxidation state of V^{5+} [38]. From these results, we can confirm that the obtained sample is V-doped NCM[39]. The charge compensation derived from vanadium doping can increase the electronic conductivity of the NCM[29].

For electrochemical tests, the loading level of the electrode was adjusted about 14.5 mg/cm^2 to meet similar condition of commercial cathode electrode. The initial charge-discharge curves (Fig. 6(a)) and cycling performance (Fig. 6(b)) of pristine and V-doped NCM samples were measured at the rate of 0.1 C and 0.5 C (202 mAh g^{-1} at 0.1 C), respectively in a potential range of 3.0–4.3 V at 25 °C. All the samples displayed typical charge-discharge profiles of Ni-rich NCM materials[40]. The pristine delivered the highest discharge capacity (204.6 mAh g^{-1}) and coulombic efficiency (89.6%). The initial discharge capacity and columbic efficiency slightly decreased with increasing the V content. It can be ascribed to the partially substituted electrochemically inactive V ions, occupying the electrochemically active transition-metal site (3b site), as reported earlier by Zhu *et al.*[22]. There was only a very slight difference between pristine and V-0.005 NCM. It was reported that the most of vanadium can enter the transition-metal site in the crystal lattice[22,28]. The small amount of vanadium dopant remaining in the NCM generates Li_3VO_4 impurity at the surface, resulting in low electrochemical activity due to reduced active materials, as shown in Fig. 2(b)[22]. However, V-doped NCM samples showed the superior cycle stability than that of pristine, as shown in Fig. 6(b). Among the V-doped NCM samples, V-0.005 NCM exhibits the best cycle retention. The capacity retention of V-0.005 NCM was 88.1% after 80 cycles. It can be ascribed

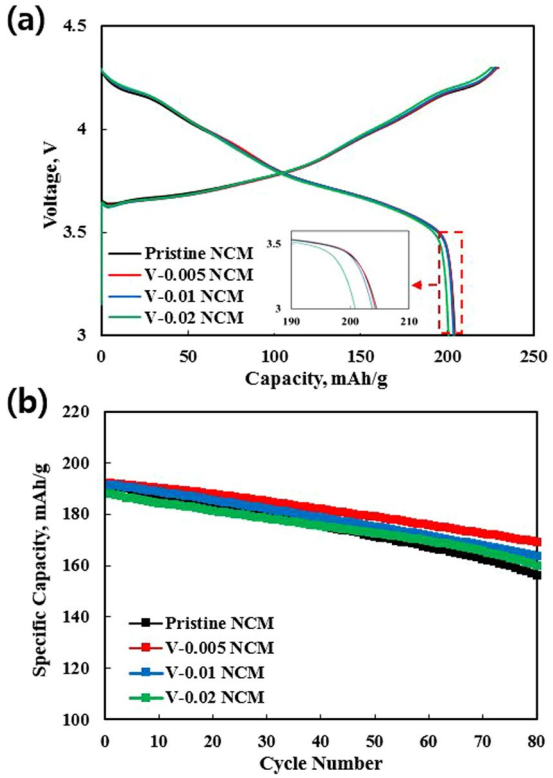

Figure 6. Initial charge-discharge curves at 0.1 C (**a**) and cycle performance at 0.5 C (**b**) of pristine and V-doped NCM samples.

Sample	Initial charge capacity (mAh g^{-1})	Initial discharge capacity (mAh g^{-1})	Initial coulombic efficiency (%)	Capacity retention after 80 cycles (%)
Pristine	228.3	204.6	89.6	81.7
V-0.005	229.5	204.4	89.1	88.1
V-0.01	228.6	203.9	89.2	85.5
V-0.02	226.1	200.9	88.8	85.2

Table 1. Electrochemical results of pristine and V-doped NCM samples.

to the bonding energies between vanadium and oxygen is stronger than that of transition metal (Ni, Co and Mn)-oxygen[22]. In addition, less Ni^{2+} ions occupy the Li^{+} sites for the NCM, leading to the NCM structure more stable. Thus, substituted vanadium ions into transition metal sites contribute to the structural stability during long-term cycling. The results are summarized in Table 1.

Figure 7 shows the rate performance of the pristine and V-doped NCM samples at different discharge current rates from 0.1 C to 2 C. The capacity of pristine NCM displayed slightly higher compared to V-doped NCM samples at low current rate from 0.1 C to 1 C. However, we can confirm that the large difference in the capacity of pristine and V-doped NCM was found at the high current density of 2 C. Although the capacity of pristine NCM is slightly higher compared to V-doped NCM, it drops off significantly with increasing current density, especially at high current density of 2 C. On the other hand, V-doped NCM samples maintained high discharge capacities at 2 C. It means that that vanadium doping is favorable to excellent rate capability derived from increasing the electronic conductivity and lattice parameters, resulting in rapid Li ion kinetics[22,41].

To investigate the effect of the vanadium doping on the electrolyte and NCM interfacial resistance, electrochemical impedance spectroscopy (EIS) were measured after 80 cycles, as shown in Fig. 8. In general, Nyquist plot consist of two semi semicircles and one slope. The electrolyte resistance (R_s) in the high frequency is not considered because the same electrolyte was used in this paper[42]. The semicircle at high frequency is related to resistance of solid electrolyte interface (R_{SEI}) and the semicircle in the middle frequency represents the charge transfer resistance (R_{ct}) at the interface between the electrode and electrolyte. The straight line with the slope of 45° at low frequencies, corresponding to the Warburg impedance, is related to Li^{+} diffusion in the bulk electrode[43]. We can observe that V-doped NCM exhibited lower R_{SEI} and R_{ct} than those of pristine NCM, as shown in Table 2. The low R_{SEI} value of V-doped NCM is closely related to the stable surface chemistry in NCM since the total bonding energy of metal-oxygen on the surface alleviates the surface degradation, as mentioned in Fig. 5. More importantly, it was reported that the R_{ct} is the key factor for the cathode impedance of cell, determining

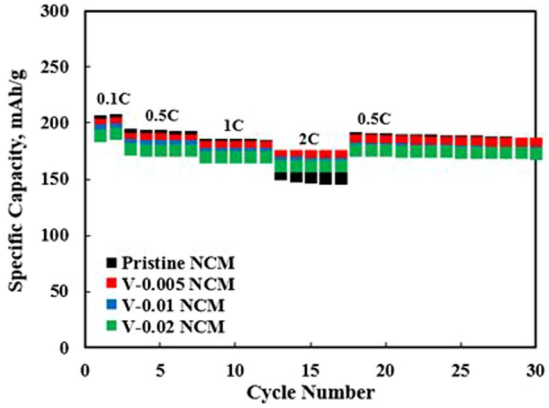

Figure 7. Rate capability of pristine and V-doped NCM samples.

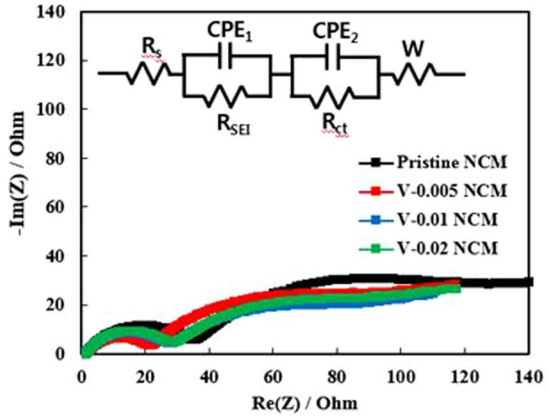

Figure 8. Nyquist plots of pristine and V-doped NCM samples after 80 cycles.

	$R_{SEI}(\Omega)$	$R_{ct}(\Omega)$
Pristine	35.838	110.58
V-0.005	20.826	85.55
V-0.01	26.660	81.43
V-0.02	27.211	94.13

Table 2. R_{SEI} and R_{ct} values of pristine and V-doped NCM samples after 80 cycles.

the electrochemical activity[44]. As shown EIS spectra, the V-0.005 NCM represented the lowest R_{ct}. Therefore, EIS result indicates that vanadium substitution can effectively suppress the increase in R_{SEI} and R_{ct} which could facilitate efficient lithium ion intercalation, resulting in superior rate capability and cyclability.

To demonstrate the reason for the improved performances of V-0.005 NCM, CV measurements were conducted. Figure 9 shows the initial CV curves of pristine and V-0.005 NCM between 3.0 and 4.3 V at a scan rate of 0.1 mV s^{-1}. The oxidation/reduction peaks of pristine and V-0.005 NCM were observed around 3.82 V/3.67 V and 3.77 V/3.69 V, respectively, corresponding to Ni^{2+}/Ni^{4+} [21]. Also, the redox peaks were observed around 4.25 V/4.14 V and 4.23 V/4.15 V, respectively, which are corresponding to Co^{3+}/Co^{4+} [40,45]. As can be seen in Fig. 9, the potential difference (ΔV) between anodic and cathodic peaks of V-0.005 NCM, indicating polarization, is smaller (0.079 V) than pristine (0.143 V). It suggests that V-0.005 NCM has a better electrochemical reversibility during the charge/discharge process[46–48]. These low R_{ct} and polarization values ensure slow capacity fading during long term cycling.

Conclusions

In this paper, V-doped $LiNi_{0.84}Co_{0.10}Mn_{0.06}O_2$ cathode material was synthesized by solid-state reaction. V-doped NCM samples exhibited better cyclic stability and rate capability (at rates as high as 2 C) compared to pristine NCM. Among them, the 0.005 M vanadium doped NCM showed the excellent structural stability and best electrochemical performances. It can be inferred that the amount of vanadium that can be substituted into the

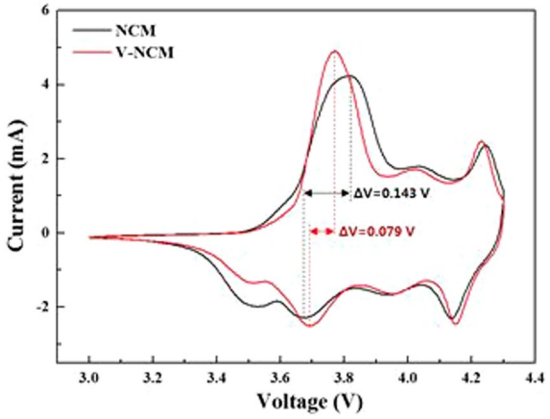

Figure 9. The cyclic voltammetry of pristine and V-doped NCM samples.

transition metal sites is limited and residual vanadium produces deleterious Li_3VO_4 impurity. The introduction of an appropriate amount of vanadium dopant not only provides smooth and rapid lithium ion insertion-extraction by large lattice parameters but also increase the electronic conductivity of NCM. More importantly, it has a positive effect on strong bonding between vanadium and oxygen, enabling remarkable structural stability. As a result, we can conclude that V-0.005 NCM can be regarded as a promising cathode for next-generation LIBs.

References

1. Myung, S.-T. *et al*. Nickl-Rich Layered Cathode Materials for Automotive Lithium-Ion Batteries: Achievements and Perspectives. *ACS Energy Lett* **2**, 196–223 (2017).
2. Schipper, F. *et al*. Recent Advances and Remaining Challenges for Lithium Ion Battery Cathodes. *J. Electrochem. Society* **164**, A6220–A6228 (2017).
3. Kondrakov, A. O. *et al*. Anisotropic Lattice Strain and Mechanical Degradation of High- and Low-Nickel NCM Cathode Materials for Li-Ion Batteries. *J. Phys. Chem. C* **121**, 3286–3294 (2017).
4. Liu, S. *et al*. Comparative studies of zirconium doping and coating on $LiNi_{0.6}Co_{0.2}Mn_{0.2}O_2$ cathode material at elevated temperatures,. *J. Power Sources* **396**, 288–296 (2018).
5. Chen, T. *et al*. The effect of gradient boracic polyanion-doping on structure, morphology, and cycling performance of Ni-rich $LiNi_{0.8}Co_{0.15}Al_{0.05}O_2$ cathode material. *J. Power Sources* **374**, 1–11 (2018).
6. Hou, P., Zhang, H., Zi, Z., Zhang, L. & Xu, X. Core-shell and concentration-gradient cathodes prepared via co-precipitation reaction for advanced lithium-ion batteries. *J. Mater. Chem. A* **5**, 4254–4279 (2017).
7. Sun, Y.-K. *et al*. A novel concentration-gradient $Li[Ni_{0.83}Co_{0.07}Mn_{0.10}]O_2$ cathode material for high-energy lithium-ion batteries. *J. Mater. Chem.* **21**, 10108–10112 (2011).
8. Li, J. *et al*. Comparison of Single Crystal and Polycrystalline $LiNi_{0.5}Mn_{0.3}Co_{0.2}O_2$ Positive Electrode Materials for High Voltage Li-Ion Cells. *J. Electrochem. Soc.* **167**, A1534–A1544 (2017).
9. Han, X., Meng, Q., Sun, T. & Sun, J. Preparation and electrochemical characterization of single-crystalline spherical $LiNi_{1/3}Co_{1/3}Mn_{1/3}O_2$ powders cathode material for Li-ion batteries. *J. Power Sources* **195**, 3047–3052 (2010).
10. Hou, P. *et al*. Improving Li^+ Kinetics and Structural Stability of Nickel-Rich Layered Cathodes by Heterogeneous Inactive-Al^{3+} Doping. *ACS Sustainable Chem. Eng.* **6**, 5653–5661 (2018).
11. Du, R. *et al*. Improved cyclic stability of $LiNi_{0.8}Co_{0.1}Mn_{0.1}O_2$ via Ti substitution with a cut-off potential of 4.5 V. *Ceramics International* **41**, 7133–7139 (2015).
12. Schipper, F. *et al*. Stabilizing nickel-rich layered cathode materials by a high-charge cation doping strategy: zirconium-doped $LiNi_{0.6}Co_{0.2}Mn_{0.2}O_2$. *J. Mater. Chem. A* **4**, 16073–16084 (2016).
13. Zhang, B., Li, L. & Zheng, J. Characterization of multiple metals (Cr, Mg) substituted $LiNi_{0.8}Co_{0.1}Mn_{0.1}O_2$ cathode materials for lithium ion battery. *J. Alloy. Comp* **520**, 190–194 (2012).
14. Li, Y. *et al*. Synthesis and characterization of Mo-doped $LiNi_{0.5}Co_{0.2}Mn_{0.3}O_2$ cathode materials prepared by a hydrothermal process. *Ceramics International* **43**, 3483–3488 (2017).
15. Wang, Y.-Y., Sun, Y.-Y., Liu, S., Li, G.-R. & Gao, X.-P. Na-Doped $LiNi_{0.8}Co_{0.15}Al_{0.05}O_2$ with Excellent Stability of Both Capacity and Potential as Cathode Materials for Li-Ion Batteries. *ACS Appl. Energy Mater* **1**, 3881–3889 (2018).
16. Kang, G.-H., Lee, K.-W., Kwon, K. & Song, J. The Effects of Incorporated Sn in Resynthesized Ni-Rich Cathode Materials on Their Lithium-Ion Battery Performance. *Metals* **7**, 395 (2017).
17. Park, K.-J. *et al*. Improved Cycling Stability of $Li[Ni_{0.90}Co_{0.05}Mn_{0.05}]O_2$ Through Microstructure Modification by Boron Doping for Li-Ion Batteries. *Adv. Energy Mater.* **8**, 1801202 (2018).
18. Liu, D., Wang, Z. & Chen, L. Comparison of structure and electrochemistry of Al- and Fe-doped $LiNi_{1/3}Co_{1/3}Mn_{1/3}O_2$. *Electrochim. Acta* **51**, 4199–4203 (2006).
19. Li, L.-J. *et al*. Synthesis, structural and electrochemical properties of $LiNi_{0.79}Co_{0.1}Mn_{0.1}Cr_{0.01}O_2$ via fast co-precipitation. *J. Alloy. Comp.* **507**, 172–177 (2010).
20. Hua, N., Wang, C., Kang, X., Wumair, T. & Han, Y. Studies of V doping for the $LiFePO_4$-based Li Ion batteries. *J. Alloy. Comp* **503**, 204–208 (2010).
21. Hu, Z. *et al*. Vanadium-doped $LiNi_{1/3}Co_{1/3}Mn_{1/3}O_2$ with decreased lithium/nickel disorder as high-rate and long-life lithium ion battery cathode. *Sci. Adv. Today* **1**, 25218 (2015).
22. Zhu, H. *et al*. The impact of vanadium substitution on the structure and electrochemical performance of $LiNi_{0.5}Co_{0.2}Mn_{0.3}O_2$. *Electrochim. Acta* **135**, 77–85 (2014).
23. Liang, C. *et al*. Site-dependent multicomponent doping strategy for Ni-rich $LiNi_{1-2y}Co_yMn_yO_2$ (y = 1/12) cathode materials for Li-ion batteries. *J. Mater. Chem. A* **5**, 25303–25313 (2017).
24. Lee, K.-S., Myung, S.-T., Amine, K., Yashiro, H. & Sun, Y.-K. Structural and Electrochemical Properties of Layered $Li[Ni_{1-2x}Co_xMn_x]O_2$ (x = 0.1–0.3) Positive Electrode Materials for Li-Ion Batteries. *J. Electrochem. Soc.* **154**, A971 (2007).

25. Zhong, W., Tu, W., Feng, S. & Xu, A. Photocatalytic H_2 evolution on CdS nanoparticles by loading FeSe nanorods as co-catalyst under visible light irradiation. *J. Alloy. Comp* **772**, 669–674 (2019).
26. Liu, Y., Shen, S., Zhang, J., Zhong, W. & Huang, X. $Cu_{2-x}Se$/CdS composite photocatalyst with enhanced visible light photocatalysis activity. *Appl. Surf. Sci.* **478**, 762–769 (2019).
27. Shaju, K. M., Rao, G. V. S. & Chodari, B. V. R. Performance of layered $Li(Ni_{1/3}Co_{1/3}Mn_{1/3})O_2$ as cathode for Li-ion batteries. *Electrochimica Acta* **48**, 145–151 (2002).
28. Lu, C. *et al*. Enhanced electrochemical performance of Li-rich $Li_{1.2}Mn_{0.52}Co_{0.08}Ni_{0.2}O_2$ cathode materials for Li-ion batteries by vanadium doping. *Electrochim. Acta* **209**, 448–455 (2016).
29. Chen, Q., Du, C., Qu, D., Zhang, X. & Tang, Z. Synthesis and characterization of Zr-doped $LiNi_{0.4}Co_{0.2}Mn_{0.4}O_2$ cathode materials for lithium ion batteries. *RSC Adv* **6**, 30194–30198 (2016).
30. Lee, J. H. *et al*. Improved performance of cylindrical hybrid supercapacitor using a ctivated carbon/niobium doped hydrogen titanate. *J. Power Sources* **301**, 348–354 (2016).
31. Zeng, D., Cabana, J., Bréger, J., Yoon, W.-S. & Grey, C. P. Cation Ordering in $Li[Ni_xMn_xCo_{(1-2\times)}]O_2$-Layered Cathode Materials: A Nuclear Magnetic Resonance (NMR), Pair Distribution Function, X-ray Absorption Spectroscopy, and Electrochemical Study. *Chem. Mater.* **19**, 6277–6289 (2007).
32. Peng, L., Zhu, Y., Khakoo, U., Chen, D. & Yu, G. Self-assembled $LiNi_{1/3}Co_{1/3}Mn_{1/3}O_2$ nanosheet cathodes with tunable rate capability. *Nano Energy* **17**, 36–42 (2015).
33. Lee, B. G. & Lee, S. H. Application of hybrid supercapacitor using granule $Li_4Ti_5O_{12}$/activated carbon with variation of current density. *J. Power Sources* **343**, 545–549 (2017).
34. Abouimrane, A. *et al*. Improved Rate Capability in a High-Capacity Layered Cathode Material via Thermal Reduction, Electrochem. *Solid-State Lett.* **14**, A126–A129 (2011).
35. Fu, Z., Hu, J., Hu, W., Yang, S. & Luo, Y. Quantitative analysis of Ni^{2+}/Ni^{3+} in $Li[Ni_xMn_yCo_z]O_2$ cathode materials: Non-linear least-squares fitting of XPS spectra. *Applied Surface Science* **441**, 1048–1056 (2018).
36. Zheng, Z. *et al*. Uniform Ni-rich $LiNi_{0.6}Co_{0.2}Mn_{0.2}O_2$ Porous Microspheres: Facile Designed Synthesis and Their Improved Electrochemical Performance. *Electrochim. Acta* **191**, 401–410 (2016).
37. Kosova, N. V., Devyatkina, E. T. & Kaichev, V. V. Optimization of Ni^{2+}/Ni^{3+} ratio in layered $Li(Ni,Mn,Co)O_2$ cathodes for better electrochemistry. *J. Power Sources* **174**, 965–969 (2007).
38. Surnev, S., Ramsey, M. G. & Netzer, F. P. Vanadium oxide surface studies. *Progress in Surface Science* **73**, 117–165 (2003).
39. Zhong, W. *et al*. Facile fabrication of alveolate $Cu_{2-x}Se$ microsheets as a new visible-light photocatalyst for discoloration of Rhodamine B. *CrystEngComm* **20**, 7851–7856 (2018).
40. Li, J., Downie, L. E., Ma, L., Qiu, W. & Dahn, J. R. Study of the Failure Mechanisms of $LiNi_{0.8}Mn_{0.1}Co_{0.1}O_2$ Cathode Material for Lithium Ion Batteries. *J. Electrochem. Soc.* **162**, A1401–A1408 (2015).
41. Lee, S. H., Kim, J. H. & Yoon, J. R. Laser Scribed Graphene Cathode for Next-Generation of High Performance Hybrid Supercapacitors. *Sci. Rep* **8**, 8179 (2018).
42. Lee, B. G., Lee, S. H., Yoon, J. R. & Ahn, H. J. Formation of holes into granule $Li_4Ti_5O_{12}$ anode for enhanced performance of hybrid supercapacitors. *Electrochim. Acta* **263**, 555–560 (2018).
43. Lee, S. H., Park, G. J., Sim, S. J., Jin, B. S. & Kim, H. S. Improved electrochemical performances of $LiNi_{0.8}Co_{0.1}Mn_{0.1}O_2$ cathode via SiO_2. *coating, J. Alloy. Comp.* **791**, 193–199 (2019).
44. Chen, C. H., Liu, J. & Amine, K. Symmetric cell approach and impedance spectroscopy of high power lithium-ion batteries. *J. Power Sources* **96**, 321–328 (2001).
45. Lu, H. *et al*. High capacity $Li[Ni_{0.8}Co_{0.1}Mn_{0.1}]O_2$ synthesized by sol–gel and co-precipitation methods as cathode materials for lithium-ion batteries. *Solid State Ionics* **249-250**, 105–111 (2013).
46. Huang, Y.-J., Gao, D.-S., Lei, G.-T., Li, Z.-H. & Su, G.-T. Synthesis and characterization of $Li(Ni_{1/3}Co_{1/3}Mn_{1/3})_{0.96}Si_{0.04}O_{1.96}F_{0.04}$ as a cathode material for lithium-ion battery. *Mater. Chem. Phys.* **106**, 354–359 (2007).
47. Li, X. *et al*. Enhanced Electrochemical Performance of Zr-Modified Layered $LiNi_{1/3}Co_{1/3}Mn_{1/3}O_2$ Cathode Material for Lithium-Ion Batteries. *ChemElectroChem* **3**, 130–137 (2016).
48. Choi, M. *et al*. The Preparation of Fe_3O_4 Thin Film and Its Electrochemical Characterization for Li-Ion Battery. *Trans. Electr. Electron. Mater* **19**, 417–422 (2018).

Acknowledgements

This work was supported by the Development Program (10067187, Development of Design and Fabrication Technology of High-Ni Based Cathode Electrode with High Energy/Safety for EV Battery) funded by the ministry of Trade, Industry and Energy (MOTIE), Korea.

Author Contributions

S.H. Lee, S.J. Sim and H.S. Kim wrote the main manuscript text. B.S. Jin and S.J. Sim carried out the sample fabrication, measurements and interpretation of the results. S.J. Sim and H.S. Kim initiated the idea of working on the present topic. S.J. Sim and S.H. Lee analyzed all experiments. All authors read and approved the final manuscript.

Additional Information

Competing Interests: The authors declare no competing interests.

Publisher's note: Springer Nature remains neutral with regard to jurisdictional claims in published maps and institutional affiliations.